Available online at www.sciencedirect.com
SCIENCE DIRECT®
Finite Elements in Analysis and Design 42 (2006) 1165–1175
FINITE ELEMENTS IN ANALYSIS AND DESIGN
www.elsevier.com/locate/finel

Modeling crack in orthotropic media using a coupled finite element and partition of unity methods

A. Asadpoure[a], S. Mohammadi[b,*], A. Vafai[a]

[a]*Department of Civil Engineering, Sharif University of Technology, Tehran, Iran*
[b]*School of Civil Engineering, University of Tehran, Tehran, Iran*

Received 3 August 2005; received in revised form 19 March 2006; accepted 28 May 2006
Available online 14 July 2006

Abstract

The problem of crack modeling in 2D orthotropic media is considered. The extended finite element method has been adopted for modeling and analyzing a crack and its domain numerically. In this method, first the finite element model without any discontinuities is created and then the two-dimensional asymptotic crack–tip displacement fields with a discontinuous function are added to enrich the finite element approximation using the framework of partition of unity. The main advantage is the ability of the method in taking into consideration a crack without any explicit meshing of the crack surfaces, and the growth of crack can readily be applied without any remeshing. Mixed-mode stress intensity factors (SIFs) are evaluated to determine the fracture properties of domain. The results of proposed method are compared with other available numerical or (semi-) analytical methods. The SIFs are obtained by means of the interaction integral (M-integral).

Keywords: Orthotropic media; Near-tip displacement; Extended finite element method (XFEM); Stress intensity factors; Crack

1. Introduction

Orthotropic materials such as composites are widely used in different branches of engineering. Since the ratio of strength to weight of such materials in many cases is higher than other conventional engineering materials, applications of these orthotropic materials have been widely expanded. Generally, composite materials are utilized in thin shell forms, which are very defect susceptible. A major type of defects that most likely to take place in these structures is cracking. Cracks can be initiated under different circumstances such as initial weakness in material strength, fatigue, yield loading and imperfection in production procedure. As a result, fracture properties and mechanics of these types of material are highly prominent; reviving the research efforts in this area by great interest.

Some analytical investigations have been reported on the fracture behavior of composite materials such as the pioneering one by Muskelishvili [1], Sih et al. [2], Tupholme [3], Viola et al. [4] and more recently Lim et al. [5] and Nobile and Carloni [6].

The analytical solution is not applicable to all problems; in particular to complicated engineering applications, whereas, the numerical approach, is the best available tool for studying general problems. There are many numerical methods utilized for modeling cracks in mechanical problems such as the boundary element method [7], the finite element method [8] and meshless methods such as the element-free Galerkin method [9]. In many mesh-less methods, simulation of arbitrary geometries and boundaries is so cumbersome. However, the finite element method is more convenient and applicable because of its ability in modeling general boundary conditions, loadings, materials and geometries. One of its main drawbacks is that elements associated with a crack must conform to crack faces. Furthermore, remeshing techniques are required to investigate and follow crack propagation patterns. To improve these drawbacks in modeling discontinuities, Belytschko et al. [10] combined FEM with the partition of unity (proposed by Melenk and Babuška [11], Duarte and Oden [12]), soon to be known as the extended finite element method (XFEM). In the XFEM, the finite element approximation is enriched with appropriate functions

* Corresponding author. Tel.: +98 21 6111 2258; fax: +98 21 6640 3808.
E-mail address: smoham@ut.ac.ir (S. Mohammadi).

0168-874X/$ - see front matter © 2006 Elsevier B.V. All rights reserved.
doi:10.1016/j.finel.2006.05.001

extracted from the fracture analysis around a crack–tip. The main advantage of the XFEM is its capability in modeling discontinuities independently, so the mesh is prepared without any considering the existence of discontinuities. In 2D isotropic media, Moës et al. [13] and Dolbow et al. [14] proposed an improvement to the work by Belytschko et al. [10]. Sukumar et al. [15] extended the method to three-dimensional problems and Sukumar and prévost [16] proposed the computer implementation.

In this study, a new method is developed for a branch of 2D orthotropic materials, complementary to the one previously proposed by Asadpoure et al. [17]. In the following sections, first fundamental formulations of a cracked plate are reviewed. Then the XFEM is briefly explained; introducing the enrichment functions based on the previous section. In order to verify the formulation and to investigate the robustness of the proposed method, stress intensity factors (SIFs) for cracked media are obtained by the method proposed by Kim and Paulino [18] and compared with other numerical or (semi-) analytical methods.

2. Basic formulation for an orthotropic medium

Consider an orthotropic medium with axes of elastic symmetry co-incident with the Cartesian co-ordinates x-, y- and z-axis. The displacement component along the z-axis and all its derivatives with respect to z are assumed to be zero. The stress–strain equations can be defined as

$$\sigma_x = C_{11}\frac{\partial u}{\partial x} + C_{12}\frac{\partial v}{\partial y}, \tag{1.1}$$

$$\sigma_y = C_{12}\frac{\partial u}{\partial x} + C_{22}\frac{\partial v}{\partial y}, \tag{1.2}$$

$$\tau_{xy} = C_{33}\left(\frac{\partial u}{\partial y} + \frac{\partial v}{\partial x}\right), \tag{1.3}$$

where C_{ij} $(i, j = 1, 2, 3)$ are the relevant components of the compliance matrix of the material in x- and y- directions. Now the set of equations for an in-plane elastostatic problem can be expressed as

$$\frac{\partial^2 u}{\partial x^2} + \alpha\frac{\partial^2 u}{\partial y^2} + 2\beta\frac{\partial^2 v}{\partial x \partial y} = 0, \tag{2.1}$$

$$\frac{\partial^2 v}{\partial x^2} + \alpha_1\frac{\partial^2 v}{\partial y^2} + 2\beta_1\frac{\partial^2 u}{\partial x \partial y} = 0, \tag{2.2}$$

where

$$\alpha = \frac{C_{66}}{C_{11}}, \quad \alpha_1 = \frac{C_{22}}{C_{33}}, \quad \beta = \frac{C_{12}+C_{33}}{2C_{11}}, \quad \beta_1 = \frac{C_{12}+C_{33}}{2C_{33}}. \tag{3}$$

Following the methodology proposed by Viola et al. [4], a transformation is applied in order to express the formulation in terms of complex functions. Eqs. (2) can be represented by

$$\frac{\partial \mathbf{\Phi}}{\partial x} + \mathbf{A}\frac{\partial \mathbf{\Phi}}{\partial y} = \mathbf{0}, \tag{4}$$

where

$$\mathbf{\Phi} = \left\{\frac{\partial u}{\partial x}, \frac{\partial u}{\partial y}, \frac{\partial v}{\partial x}, \frac{\partial v}{\partial y}\right\}^{\mathrm{T}}, \tag{5}$$

$$\mathbf{A} = \begin{pmatrix} 0 & \alpha & 2\beta & 0 \\ -1 & 0 & 0 & 0 \\ 2\beta_1 & 0 & 0 & \alpha_1 \\ 0 & 0 & -1 & 0 \end{pmatrix}. \tag{6}$$

Eigenvalues of the matrix $\mathbf{A}$ can be obtained by

$$\lambda^4 + 2a_1\lambda^2 + a_2 = 0 \tag{7}$$

with

$$a_1 = \frac{(\alpha + \alpha_1 - 4\beta\beta_1)}{2}, \tag{8.1}$$

$$a_2 = \alpha\alpha_1, \tag{8.2}$$

where λ is the Eigenvalue of matrix $\mathbf{A}$. Two types of orthotropic materials can be defined, $a_1 > \sqrt{a_2}$ (type I) and $|a_1| < \sqrt{a_2}$ (type II); based on the existence of the real part of the solution. The first type of orthotropic materials was studied by Asadpoure et al. [17], and only the type II is considered in this paper. The basic complex variables can then be written as

$$z_1 = \left(x - \frac{\gamma_1}{\gamma_1^2+\gamma_2^2}y\right) + i\left(\frac{\gamma_2}{\gamma_1^2+\gamma_2^2}y\right), \tag{9.1}$$

$$z_2 = \left(x + \frac{\gamma_1}{\gamma_1^2+\gamma_2^2}y\right) + i\left(\frac{\gamma_2}{\gamma_1^2+\gamma_2^2}y\right), \tag{9.2}$$

where

$$\gamma_1 = \left[\frac{1}{2}(\sqrt{a_2} + a_1)\right]^{1/2}, \tag{10.1}$$

$$\gamma_2 = \left[\frac{1}{2} + (\sqrt{a_2} - a_1)\right]^{1/2}. \tag{10.2}$$

Viola et al. [4] explained the procedure of obtaining the complex variables and functions. Now, consider an infinite orthotropic plate, consisting of a traction free line crack, which is subjected to uniform biaxial (T and kT) and shear (S) loads at infinity. Fig. 1 shows the crack geometry, loading conditions and the Cartesian and polar co-ordinates utilized in this study.

Neglecting the velocity of the crack propagation for the present static case, the basic solution proposed by Viola et al. [4] results in the following displacement fields in x

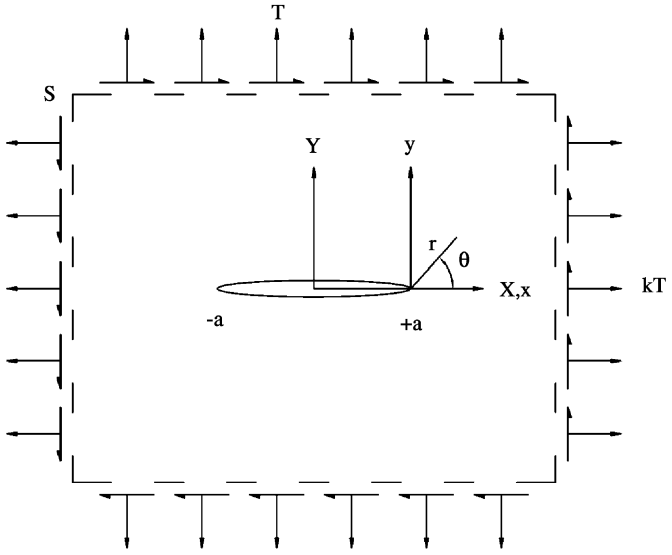

Fig. 1. Crack geometry, loading condition and global and local co-ordinates.

and y directions:

$$\begin{aligned} u = & -2\beta[(p_3A_1 - p^4B_1 + p_4B_2)Y_1 \\ & + (p_3B_1 + p_4A_1)X_1 + p_3B_2X_2] \\ & + \frac{\beta T}{C_{33}D_1}\{(p_3k_6 + p_4k_5)[2(a + r\cos\theta) \\ & - \sqrt{2ar}(\sqrt{c_1(\theta)}\cos\theta_1/2 + \sqrt{c_2(\theta)}\cos\theta_2/2)] \\ & - (p_3k_5 + p_4k_5)\sqrt{2ar}(\sqrt{c_1(\theta)}\sin\theta_1/2 \\ & - \sqrt{c_2(\theta)}\sin\theta_2/2)\} \\ & + \frac{\beta S}{C_{33}D_1}\{(p_3k_3 + p_4k_4)[X_1 - X_2 \\ & + \sqrt{2ar}(\sqrt{c_2(\theta)}\cos\theta_2/2 - \sqrt{c_1(\theta)}\cos\theta_1/2)] \\ & - (p_3k_4 + p_4k_3)[2Y_1 - \sqrt{2ar}(\sqrt{c_1(\theta)}\sin\theta_1/2 \\ & + \sqrt{c_2(\theta)}\sin\theta_2/2)]\}, \end{aligned} \tag{11}$$

$$\begin{aligned} v = & -[(\gamma_1A_1 - \gamma_2B_1 - \gamma_2B_2)Y_1 + (\gamma_2A_1 + \gamma_1B_2)X_1 \\ & - \gamma_1B_2X_2] + \frac{T}{2C_{33}D_1}\{(\gamma_1k_6 + \gamma_2k_5)[(X_1 - X_2) \\ & + \sqrt{2ar}(\sqrt{c_1(\theta)}\cos\theta_2/2 - \sqrt{2ar}\cos\theta_2/2)] \\ & + (\gamma_1k_5 - \gamma_2k_6)[2Y_1 - \sqrt{2ar}(\sqrt{c_1(\theta)}\sin\theta_1/2 \\ & + \sqrt{c_2(\theta)}\sin\theta_2/2)]\} + \frac{S}{2C_{33}D_1}\{(\gamma_1k_3 - \gamma_2k_4) \\ & \times [2(a + r\cos\theta) - \sqrt{2ar}(\sqrt{c_1(\theta)}\cos\theta_1/2 \\ & + \sqrt{c_2(\theta)}\cos\theta_2/2)] + (\gamma_2k_3 + \gamma_1k_4)\sqrt{2ar} \\ & \times (\sqrt{c_1(\theta)}\sin\theta_1/2 + \sqrt{c_2(\theta)}\sin\theta_2/2)\}, \end{aligned} \tag{12}$$

where

$$\begin{aligned} & p_1 + \mathrm{i}p_2 = \frac{(\gamma_1 + \mathrm{i}\gamma_2)}{\alpha + (\gamma_1 + \mathrm{i}\gamma_2)^2}, \\ & p_3 + \mathrm{i}p_4 = (\gamma_1 + \mathrm{i}\gamma_2)(p_1 - \mathrm{i}p_2), \end{aligned} \tag{13.1}$$

$$k_1 = \frac{C_{12} - 2\beta p_3C_{11}}{C_{33}}, \quad k_2 = 2\beta p_4\frac{C_{11}}{C_{33}}, \tag{13.3}$$

$$k_3 = \frac{C_{22} - 2\beta p_3C_{12}}{C_{33}}, \quad k_4 = 2\beta p_4\frac{C_{12}}{C_{33}}, \tag{13.4}$$

$$k_5 = 2\beta p_2 - \gamma_2, \quad k_6 = 2\beta p_1 - \gamma_1 \tag{13.5}$$

with

$$X_1 = (a + r\cos\theta) - \gamma_1 l^2 r\sin\theta, \tag{14.1}$$

$$X_2 = (a + r\cos\theta) + \gamma_1 l^2 r\sin\theta, \tag{14.2}$$

$$Y_1 = \gamma_2 l^2 r\sin\theta, \tag{14.3}$$

$$A_1 = \frac{(k_3k - k_1)T}{C_{33}(k_1k_4 - k_2k_3)}, \tag{14.4}$$

$$\begin{aligned} B_1 = & \frac{S}{2C_{33}k_6} \\ & + \frac{T}{2C_{33}k_6}\frac{[k(k_4k_6 - k_3k_5) + (k_1k_5 - k_2k_6)]}{(k_1k_4 - k_2k_3)}, \end{aligned} \tag{14.5}$$

$$\begin{aligned} B_2 = & -\frac{S}{2C_{33}k_6} \\ & + \frac{T}{2C_{33}k_6}\frac{[k(k_4k_6 - k_3k_5) - (k_1k_5 + k_2k_6)]}{(k_1k_4 - k_2k_3)}, \end{aligned} \tag{14.6}$$

$$D_1 = k_3k_6 - k_4k_5, \tag{14.7}$$

and

$$\begin{aligned} & c_j(\theta) = (\cos^2\theta + l^2\sin^2\theta + (-1)^j l^2\sin 2\theta)^{1/2}, \\ & l^2 = (\gamma_1^2 + \gamma_2^2)^{-1}, \quad j = 1, 2, \end{aligned} \tag{15}$$

$$\theta_j = arctg\left(\frac{\gamma_2 l^2\sin\theta}{\cos\theta + (-1)^j\gamma_1 l^2\sin\theta}\right), \quad j = 1, 2. \tag{16}$$

It is noted that the displacement fields in Eqs. (11)–(12) are only valid for $r/a < 1$; near the crack–tip.

3. Extended finite element method

The XFEM was originally proposed by Belytschko and Black [10]. They enriched the finite element approximation by adding some discontinuous functions to the approximation. The procedure of enriching the approximation was performed using the partition of unity method [11,12]. For modeling a curved crack, Belytschko and Black [10] separated the crack into a set of straight segments and mapped each one of them into the first segment alignment. For a long curved crack, this procedure becomes very complex. Moës et al. [13] improved the method by introducing the generalized Heaviside function for modeling the crack surfaces. Therefore, the cumbersome mapping procedure is not required and the jump in the displacement (strong discontinuity) across the crack faces (not the crack–tip) can be readily modeled with the new function.

In the XFEM, the numerical model is prepared in two steps. In the first step, the mesh is generated without considering the existence of cracks or any discontinuities. Then, with the help

of partition of unity method and discontinuous functions, the FEM mesh is locally enriched in order to capture the effect of cracks or other discontinuities within the mesh. Because of the range of validity of the analytical solution of displacement fields around the crack–tip (in Eqs. (11)–(12), $r/a < 1$), the size of elements containing a crack–tip must be restricted with respect to the crack length and the gradient of stress field around the crack–tip.

3.1. Preliminary equations

For a point $\mathbf{x}$ locating within a domain, the extended finite element approximation for the enriched displacement field can be defined by

$$\mathbf{u}^h(\mathbf{x}) = \sum_{\substack{I \\ n_I \in \mathbf{N}}} \phi_I(\mathbf{x})\mathbf{u}_I + \sum_{\substack{J \\ n_J \in \mathbf{N}^g}} \phi_J(\mathbf{x})\psi(\mathbf{x})\mathbf{a}_J, \tag{17}$$

where $\mathbf{N}$ is the set of all nodes in the domain, n_i is the node I, ϕ_I is the shape function associated to node I, $\mathbf{u}_I$ is the vector of regular degrees of nodal freedom in finite element method, $\mathbf{a}_J$ is the added set of degrees of freedom to the standard finite element model, $\mathbf{N}^g$ is the set of nodes that the discontinuity is in its influence (support) domain and $\psi(\mathbf{x})$ is the discontinuous function. Fig. 2 shows the influence domain for a typical node in an arbitrary discretization of a domain. Only those nodes whose influence domains are cut by a crack will be enriched. In Eq. (17), the first expression in the right-hand side is the classical finite element expression to approximate the displacement and second one is the enriched approximation to include the effects of discontinuities in the finite element method.

3.2. Modeling crack

For modeling a crack in the XFEM, Eq. (17) can be re-written as [13]

$$\begin{aligned}\mathbf{u}^h(\mathbf{x}) = &\sum_{\substack{I \\ n_I \in \mathbf{N}}} \phi_I(\mathbf{x})\mathbf{u}_I + \sum_{\substack{J \\ n_J \in \mathbf{N}^g}} \mathbf{b}_J \phi_J(\mathbf{x})H(\mathbf{x}) \\ &+ \sum_{k \in \mathbf{K}^1} \phi_k(\mathbf{x}) \left(\sum_l \mathbf{c}_k^{l1} F_l^1(\mathbf{x}) \right) \\ &+ \sum_{k \in \mathbf{K}^2} \phi_k(\mathbf{x}) \left(\sum_l \mathbf{c}_k^{l2} F_l^2(\mathbf{x}) \right),\end{aligned} \tag{18}$$

where $\mathbf{b}_J$ is the vector of additional degrees of nodal freedom for modeling crack faces (not crack–tips), $\mathbf{c}_k$ is the vector of additional degrees of nodal freedom for modeling crack–tips, $\mathbf{N}^g$ is the set of nodes that have crack face (but not crack–tip) in their support domain, $F_l^i(\mathbf{x})$, $(i = 1, 2.)$, are crack–tip enrichment functions and $\mathbf{K}^1$ and $\mathbf{K}^2$ are sets of nodes associated with crack–tip 1 and 2 in their influence domain, respectively. In Eq. (18), $H(\mathbf{x})$ is the generalized Heaviside function. This function was originally proposed by Moës et al. [13] to model the discontinuity in the displacement in both sides of the crack

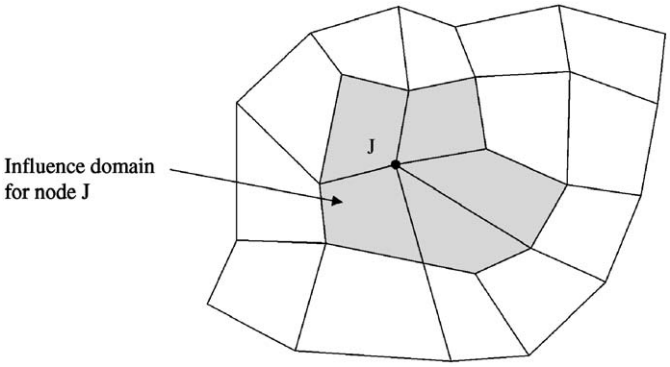

Fig. 2. Definition of the influence (support) domain for a typical node J in an arbitrary finite element mesh.

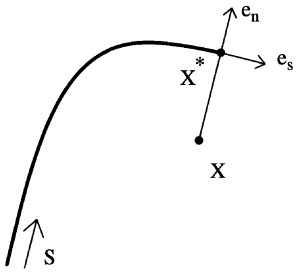

Fig. 3. Unit tangential and normal vectors for the Heaviside function.

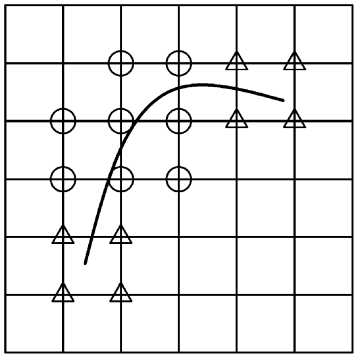

Fig. 4. Node selection for enrichment; nodes marked by triangles are enriched by crack–tip functions and the circled ones are enriched by the Heaviside function.

faces and takes the value $+1$ if $\mathbf{x}$ is above the crack and -1, otherwise. If $\mathbf{x}^*$ is the nearest point on the crack to $\mathbf{x}$ (see Fig. 3) and $\mathbf{e_n}$ is the unit vector normal to the crack alignment in which $\mathbf{e_s} \times \mathbf{e_n} = \mathbf{e_z}$ ($\mathbf{e_s}$ is the unit tangential vector and $\mathbf{e}_z$ is the outward normal to the surface), then

$$H(\mathbf{x}) = \begin{cases} +1; & \text{if}(\mathbf{x} - \mathbf{x}^*).\mathbf{e_n} > 0, \\ -1; & \text{otherwise.} \end{cases} \tag{19}$$

Fig. 4 illustrates a part of a domain containing a crack with an arbitrary geometry. In this figure, the circled nodes are enriched with the Heaviside function and nodes marked by triangles are enriched with crack–tip functions.

Crack–tip enrichment functions are obtained from the analytical solution for displacement in the vicinity of a crack–tip. These functions must span the possible displacement space that may be occurred in the analytical solution. Therefore, from Eqs. (11)–(12), it can be concluded that the functions having preceding properties are as

$$\{F_l(r,\theta)\}_{l=1}^{4} = \left\{\sqrt{r}\cos\frac{\theta_1}{2}\sqrt{c_1(\theta)},\ \sqrt{r}\cos\frac{\theta_2}{2}\sqrt{c_2(\theta)},\ \sqrt{r}\sin\frac{\theta_1}{2}\sqrt{c_1(\theta)},\ \sqrt{r}\sin\frac{\theta_2}{2}\sqrt{c_2(\theta)}\right\}. \quad (20)$$

In Eq. (20), the third and forth functions in the right-hand side of the equation are discontinuous across the crack faces while the others remain continuous. Although, Eq. (20) contains similar terms as to the crack–tip enrichment functions proposed by Asadpoure et al. [17], fundamentally different mathematical definitions are used for the definition of θ_1, θ_2, $c_1(\theta)$ and $c_2(\theta)$ functions. They proposed the following parameters and functions when $a_1 > \sqrt{a_2}$ [17]:

$$c_i(\theta) = \left(\cos^2\theta + \frac{\sin^2\theta}{p_j^2}\right)^{1/2}, \quad j = 1, 2, \quad (21)$$

$$\theta_j = tg^{-1}\left(\frac{y}{p_j x}\right) = tg^{-1}\left(\frac{tg\theta}{p_j}\right), \quad (22)$$

where

$$p_1 = \left(A - \left(A^2 - \frac{C_{22}}{C_{11}}\right)^{1/2}\right)^{1/2},$$

$$p_2 = \left(A + \left(A^2 - \frac{C_{22}}{C_{11}}\right)^{1/2}\right)^{1/2}, \quad (23)$$

and

$$A = \frac{1}{2}\left[\frac{C_{66}}{C_{11}} + \frac{C_{22}}{C_{66}} - \frac{(C_{12}+C_{66})^2}{C_{11}C_{66}}\right]. \quad (24)$$

The discrete system of linear equations in the XFEM in global form can be written as (Sukumar and prévost [16])

$$\mathbf{Kd} = \mathbf{f}, \quad (25)$$

where $\mathbf{K}$ is the stiffness matrix, $\mathbf{d}$ is the vector of degrees of nodal freedom (for both classical and enriched ones) and $\mathbf{f}$ is the vector of external force. The global matrix and vectors are calculated by assembling matrices and vectors of each element. $\mathbf{K}$ and $\mathbf{f}$ for each element are defined as

$$\mathbf{K}_{ij}^{e} = \begin{bmatrix} \mathbf{K}_{ij}^{uu} & \mathbf{K}_{ij}^{ua} & \mathbf{K}_{ij}^{ub} \\ \mathbf{K}_{ij}^{au} & \mathbf{K}_{ij}^{aa} & \mathbf{K}_{ij}^{ab} \\ \mathbf{K}_{ij}^{bu} & \mathbf{K}_{ij}^{ba} & \mathbf{K}_{ij}^{bb} \end{bmatrix}, \quad (26.1)$$

$$\mathbf{f}_i^{e} = \{\mathbf{f}_i^{u}\ \ \mathbf{f}_i^{a}\ \ \mathbf{f}_i^{b1}\ \ \mathbf{f}_i^{b2}\ \ \mathbf{f}_i^{b3}\ \ \mathbf{f}_i^{b4}\}^{T}, \quad (26.2)$$

where

$$\mathbf{K}_{ij}^{rs} = \int_{\Omega^e} (\mathbf{B}_i^r)^T \mathbf{D}\mathbf{B}_j^s \, d\Omega \quad (r, s = u, a, b), \quad (27.1)$$

$$\mathbf{f}_i^{u} = \int_{\partial\Omega_t^h \cap \partial\Omega^e} \varphi_i \bar{\mathbf{t}} \, d\Gamma + \int_{\Omega^e} \varphi_i \mathbf{b} \, d\Omega, \quad (27.2)$$

$$\mathbf{f}_i^{a} = \int_{\partial\Omega_t^h \cap \partial\Omega^e} \varphi_i H \bar{\mathbf{t}} \, d\Gamma + \int_{\Omega^e} \varphi_i H \mathbf{b} \, d\Omega, \quad (27.3)$$

$$\mathbf{f}_i^{b\alpha} = \int_{\partial\Omega_t^h \cap \partial\Omega^e} \varphi_i F_\alpha \bar{\mathbf{t}} \, d\Gamma + \int_{\Omega^e} \varphi_i F_\alpha \mathbf{b} \, d\Omega \quad (\alpha = 1, 2, 3 \text{ and } 4), \quad (27.4)$$

where Ω^e is an element, Ω^h is an element with a crack lying along its edges, $\partial\Omega$ denotes the boundary of the domain Ω, $\bar{\mathbf{t}}$ is the traction and $\mathbf{b}$ is the body force. In Eqs. (23), $\mathbf{B}$ is the matrix of shape function derivatives,

$$\mathbf{B}_i^{u} = \begin{bmatrix} \varphi_{i,x} & 0 \\ 0 & \varphi_{i,y} \\ \varphi_{i,y} & \varphi_{i,x} \end{bmatrix}, \quad (28.1)$$

$$\mathbf{B}_i^{a} = \begin{bmatrix} (\varphi_i H)_{,x} & 0 \\ 0 & (\varphi_i H)_{,y} \\ (\varphi_i H)_{,y} & (\varphi_i H)_{,x} \end{bmatrix}, \quad (28.2)$$

$$\mathbf{B}_i^{b} = [\mathbf{B}_i^{b1}\ \ \mathbf{B}_i^{b2}\ \ \mathbf{B}_i^{b3}\ \ \mathbf{B}_i^{b4}], \quad (28.3)$$

$$\mathbf{B}_i^{\alpha} = \begin{bmatrix} (\varphi_i F_\alpha)_{,x} & 0 \\ 0 & (\varphi_i F_\alpha)_{,y} \\ (\varphi_i F_\alpha)_{,y} & (\varphi_i F_\alpha)_{,x} \end{bmatrix} \quad (\alpha = 1, 2, 3 \text{ and } 4). \quad (28.4)$$

Because the ordinary Gaussian rules do not accurately calculate the integration of enrichment functions in elements cut by a crack, Dolbow [14] proposed two methods to overcome this numerical difficulty. The first method is to subdivide the element at both sides of the crack into subtriangles whose edges are adapted to crack faces and the second one is to subdivide the element into subquads. Both methods are illustrated in Fig. 5. In the first method, if values of $A^-/(A^+ + A^-)$ and $A^+/(A^+ + A^-)$, where A^+ and A^- are the area of the influence

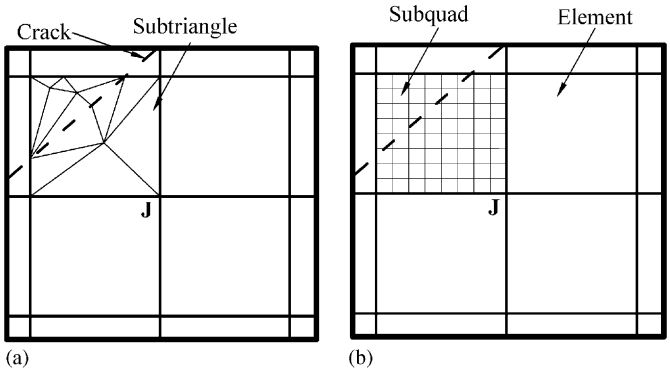

Fig. 5. Two methods for partitioning the cracked element: (a) the cracked element is subdivided into subtriangles; (b) the cracked element is subdivided into subsubquads.

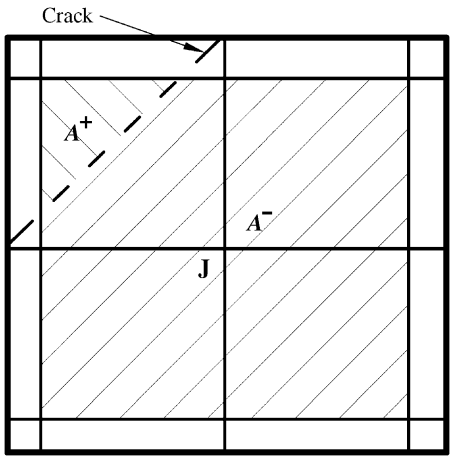

Fig. 6. A^+ and A^- for node J in its influence domain.

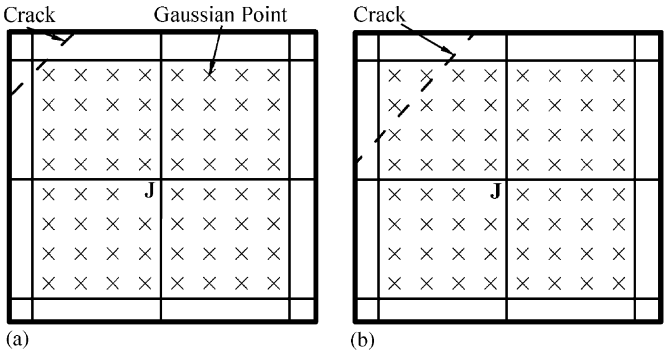

Fig. 7. (a) Node J must not be enriched because Gaussian points of its support domain are not present at both sides of the crack, (b) node J must be enriched since there are Gaussian points at both sides of the crack.

domain of a node above and below the crack, respectively (see Fig. 6) (proposed by Dolbow [14]), are smaller than an allowable tolerance value, the node must not be enriched. The tolerance value proposed by Dolbow [14] is 0.01%. In the second method, a node is enriched if there exist Gaussian points at both sides of the crack in the influence domain of the crack. Fig. 7 shows a mesh that contains a crack while the second method was applied. Although the crack cuts the element in Fig. 7(a), node J must not be enriched because there is no Gaussian point above the crack. In contrary, node J in Fig. 7(b) has to be enriched. It should be noted that in this paper, only the second method is utilized.

4. Numerical examples

In this section some examples are presented. For comparing the results, stress intensity factors (SIFs) and J-integral are calculated and compared. These parameters are among the best parameters for determination of the path of crack propagation. In this section, SIFs and J-integral are obtained by the method proposed by Kim and Paulino [19]. In the subsequent plane stress examples, the following parameters, being the function of independent engineering constants (E_{ij}, v_{ij}, G_{ij}, $i, j = 1, 2.$), would be used:

$$E = \sqrt{E_{11}E_{22}}, \quad v = \sqrt{v_{12}v_{21}},$$
$$\delta^4 = \frac{E_{11}}{E_{22}} = \frac{v_{12}}{v_{21}}, \quad \kappa_0 = \frac{E}{2G_{12}} - v, \tag{29}$$

where E is the efficient Young's modulus, v is the effective Poisson's ratio, δ^4 is the stiffness ratio and κ_0 is the shear parameter.

In all examples, elements containing a crack are partitioned into 10 subquads and a 2×2 Gaussian rule is utilized for integrations in each one; while, a 2×2 Gaussian rule is applied in calculating regular finite element parameter.

4.1. Plate with a crack parallel to material axes of orthotropy

In this example, a crack aligned along the axis of orthotropy in the center of a plate is studied. At edges parallel to the crack, a fixed-grip loading or constant traction is applied. The constant stress is obtained by utilizing a uniform stress ($\sigma = 1$) and the fixed-grip loading is obtained by a load equivalent to strain ($\varepsilon_0 = 1$) in the corresponding uncracked plate. Geometry and boundary conditions for the problem are illustrated in Fig. 8.

In the FEM discretization, 2116 nodes with 2025 four-noded quadrilateral elements are used (Fig. 9). The size of crack–tip element is one-sixteenth of the crack length, i.e. $h_e/a = 1/8$. Stress intensity factors are calculated and compared with those reported by Kim and Paulino [19], using a total of 2001 elements and 5851 nodes, as shown in Table 1.

Table 2 shows the rate of convergence for various integration domain sizes (r_d) for enrichment with and without crack–tip enrichment functions. As provided in Table 2 small domain sizes

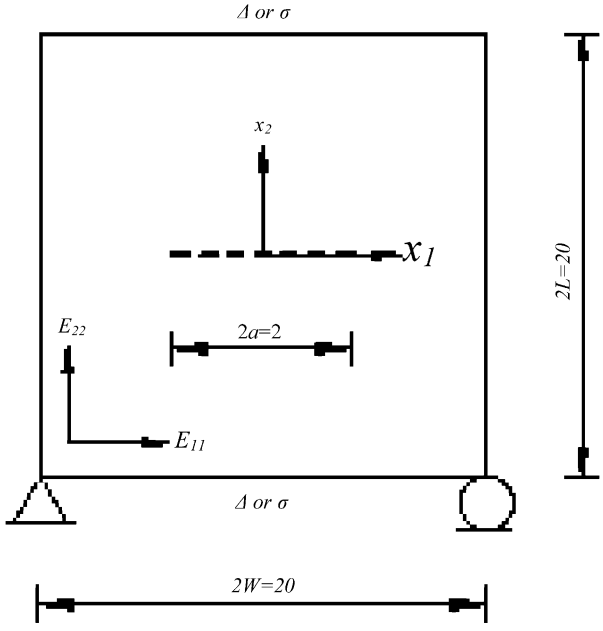

Fig. 8. Geometry and boundary conditions for a plate with a crack parallel to material axis of orthotropy.

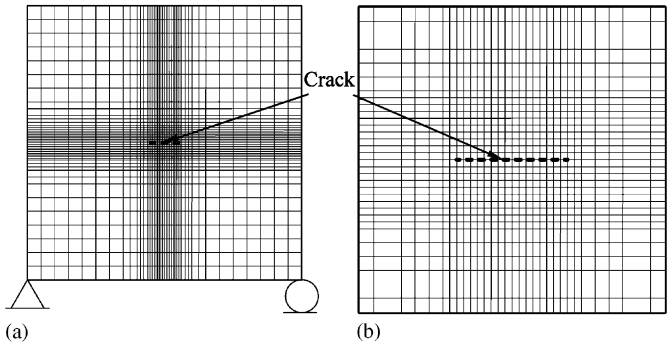

Fig. 9. The discretizated model for a plate with a crack parallel to material axis of orthotropy: (a) whole view of FEM discretization model; (b) details of discretization around the crack–tip.

Table 1
Values of normalized SIFs for a plate with a crack parallel to material axis of orthotropy

Method	$\overline{K}_{\mathrm{I}}$	$\overline{K}_{\mathrm{II}}$
Kim and Paulino [19]	0.997	0
Proposed method	1.018	0

$\overline{K}_{\mathrm{I}} = K_{\mathrm{I}}/\sigma\sqrt{\pi a}$ and $\overline{K}_{\mathrm{II}} = K_{\mathrm{II}}/\sigma\sqrt{\pi a}$ for the applied uniform stress and $\overline{K}_{\mathrm{I}} = K_{\mathrm{I}}\delta^2/\varepsilon_0 E\sqrt{\pi a}$ and $\overline{K}_{\mathrm{II}} = K_{\mathrm{II}}\delta^2/\varepsilon_0 E\sqrt{\pi a}$ for fixed-grip loading.

Table 2
Comparison of normalized SIFs with and without crack–tip functions for a plate with a crack parallel to material axis of orthotropy

Relative domain size (r_{d}/a)	Without crack–tip function		With crack–tip function	
	$\overline{K}_{\mathrm{I}}$	$\overline{K}_{\mathrm{II}}$	$\overline{K}_{\mathrm{I}}$	$\overline{K}_{\mathrm{II}}$
0.25	0.966	0	1.018	0
0.5	1.014	0	1.017	0
1	1.015	0	1.017	0
2	1.016	0	1.018	0

In the table, $\overline{K}_{\mathrm{I}} = K_{\mathrm{I}}/\sigma\sqrt{\pi a}$ and $\overline{K}_{\mathrm{II}} = K_{\mathrm{II}}/\sigma\sqrt{\pi a}$ for the applied uniform stress and $\overline{K}_{\mathrm{I}} = K_{\mathrm{I}}\delta^2/\varepsilon_0 E\sqrt{\pi a}$ and $\overline{K}_{\mathrm{II}} = K_{\mathrm{II}}\delta^2/\varepsilon_0 E\sqrt{\pi a}$ for fixed-grip loading.

Table 3
Comparison of normalized SIFs for the proposed and isotropic enrichment functions when several meshes are used

Number of elements	Number of DOF	Proposed enrichment functions		Isotropic enrichment functions	
		$\overline{K}_{\mathrm{I}}$	$\overline{K}_{\mathrm{II}}$	$\overline{K}_{\mathrm{I}}$	$\overline{K}_{\mathrm{II}}$
2025	4278	1.018	0	1.021	0
784	1712	1.017	0	1.019	0
400	904	1.017	0	1.016	0

$\overline{K}_{\mathrm{I}} = K_{\mathrm{I}}/\sigma\sqrt{\pi a}$ and $\overline{K}_{\mathrm{II}} = K_{\mathrm{II}}/\sigma\sqrt{\pi a}$.

cannot be used without the inclusion of crack–tip enrichment functions and in order to compensate for the local effects of the crack–tip, larger domains are preferred.

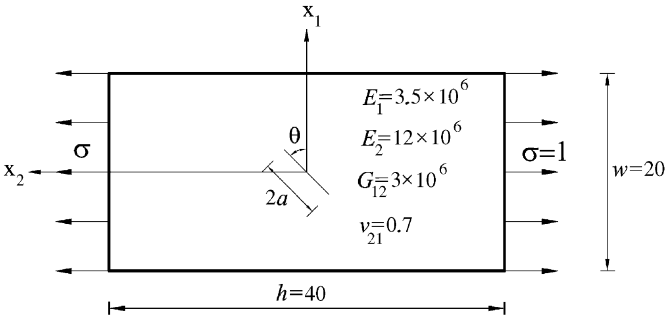

Fig. 10. Geometry of a plate with a slanted crack under remote tension.

By including crack–tip enrichment functions, higher rates of convergence are anticipated, even for smaller domain sizes around the crack–tip. Numerical results show that when $r_{\mathrm{d}}/a = 0.5$, the values of SIFs are independent from the domain size.

To investigate the effect of number of elements in the numerical analysis, some coarser meshes are utilized and the results are given in Table 3. In this table, the results for SIFs are compared when isotropic enrichment functions [14] and the proposed method are applied. As shown in Table 3, the results for both methods are different 0.2% and the values of the mode I stress intensity factors are more stable than the other one.

4.2. Slanted crack

In this example the proposed method is applied to a slanted crack of length $2a = 2\sqrt{2}$ located in a finite two-dimensional orthotropic plate under constant applied tension (Fig. 10). The angle of the crack with respect to x_1-axis is 45°.

Two thousand five hundred and one nodes and 2400 elements are utilized in the FEM discretization (Fig. 11). Element sizes are smaller in the vicinity of the crack than the other parts of the discretized model and the crack–tip size is one-sixteenth of the crack length.

Stress intensity factors are compared with results reported by Sih et al. [2], Atluri et al. [20], Wang et al. [21] and Kim and Paulino [18]. According to Table 4, the results are different 2.6% for K_{I} and 3.6% for K_{II} in comparison to Sih et al. [2].

Fig. 12 illustrates the normalized SIFs corresponding to different crack angles, θ, with respect to x_1-axis. By increasing the crack angle, mode I stress intensity factor reduces; however, mode II stress intensity factor increases and reaches its maximum value at $\theta = 45°$, and then decreases. It is worth noting that for all crack alignments, the same discretized model is applied and it shows the capability of XFEM in modeling various crack geometries with the same FEM model.

In Fig. 13, values of SIFs corresponding to different sizes of the integration domain are illustrated. The results are expected to be domain-independent when the domain size reaches to about 0.75 of half the crack length.

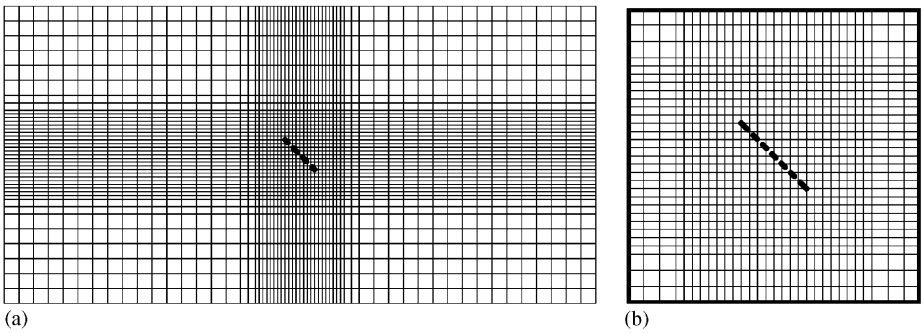

Fig. 11. FEM discretization of a plate with a slanted crack under remote tension: (a) whole view of FEM discretization model; (b) details of discretization around the crack–tip.

Table 4
SIFs in an orthotropic plate with a slanted crack under uniform remote tensile loading

Method		K_{I}	K_{II}
Sih et al. [2]		1.0539	1.0539
Atluri et al. [20]		1.0195	1.0795
Wang et al. [21]		1.023	1.049
Kim and Paulino [18]	MCC	1.067	1.044
	DCT	1.077	1.035
Proposed method		1.081	1.092

If isotropic enrichment functions (proposed by Dolbow [14]) are applied in the case that $\theta=45°$, values for mixed mode SIFs are obtained as 1.083 and 1.074 for modes I and II, respectively. For further investigation and comparison of the proposed and isotropic enrichment functions, the rate of convergence of SIFs for both enrichment functions is studied for a crack inclination $\theta=30°$, resulting in the evaluated SIFs given in Table 5. On the contrary to the previous example, the differences of SIFs calculated from both methods are not negligible and may exceed up to 3.5%. When a coarser mesh is utilized, differences of SIFs

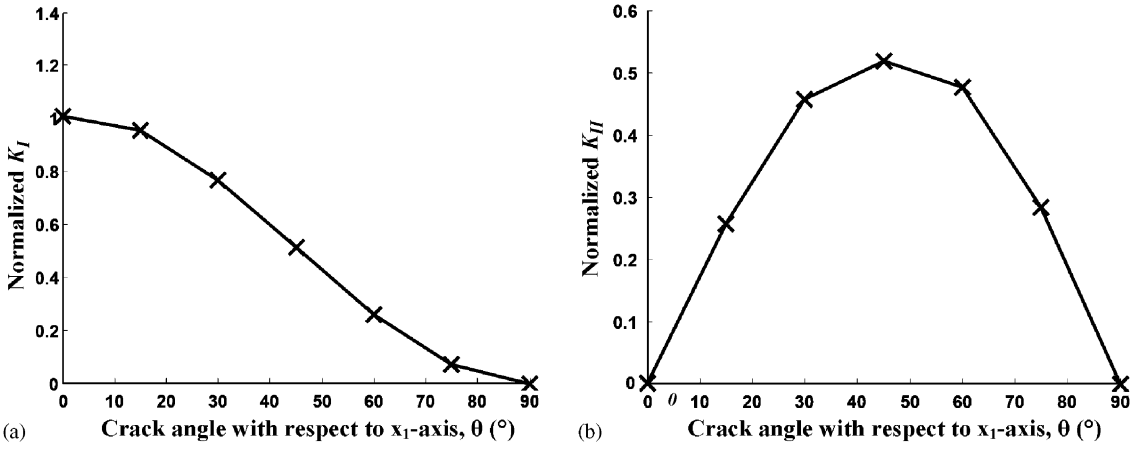

Fig. 12. Normalized SIFs corresponding to different crack angles for a plate with a slanted crack subjected to remote tension: (a) normalized SIF for mode I; (b) normalized SIF for mode II. ($\overline{K}_{\mathrm{I}}=K_{\mathrm{I}}/\sigma\sqrt{\pi a}$ and $\overline{K}_{\mathrm{II}}=K_{\mathrm{II}}/\sigma\sqrt{\pi a}$).

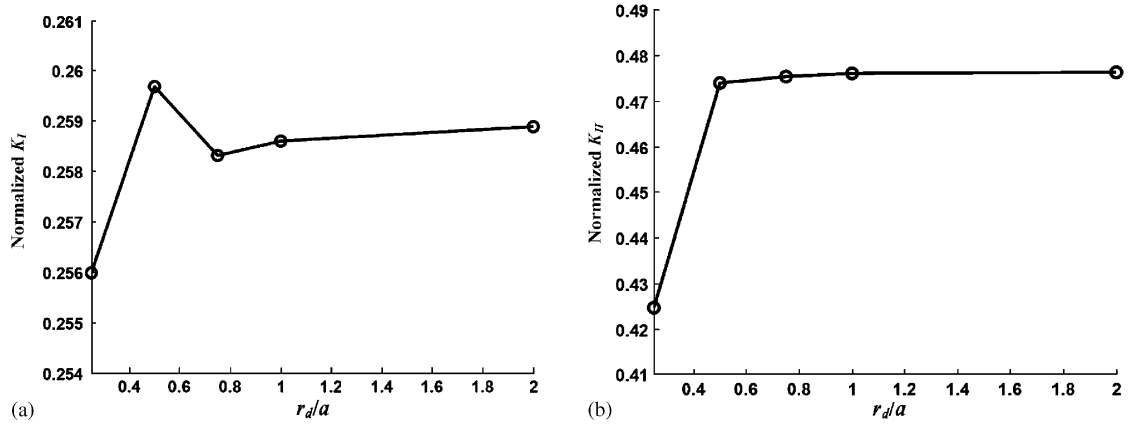

Fig. 13. Rate of convergence of SIFs with $\theta=60°$ with respect to relative domain size in a plate with a slanted crack under remote tension: (a) normalized SIF for mode I; (b) normalized SIF for mode II. ($\overline{K}_{\mathrm{I}}=K_{\mathrm{I}}/\sigma\sqrt{\pi a}$ and $\overline{K}_{\mathrm{II}}=K_{\mathrm{II}}/\sigma\sqrt{\pi a}$).

Table 5
Comparison of normalized SIFs with $\theta = 30°$ for the proposed and isotropic enrichment functions when several meshes are used

Number of elements	Number of DOF	Proposed enrichment functions		Isotropic enrichment functions	
		$\overline{K}_{\mathrm{I}}$	$\overline{K}_{\mathrm{II}}$	$\overline{K}_{\mathrm{I}}$	$\overline{K}_{\mathrm{II}}$
2400	5112	0.769	0.456	0.764	0.439
1496	3260	0.768	0.456	0.763	0.439
816	1836	0.798	0.482	0.776	0.441

$\overline{K}_{\mathrm{I}} = K_{\mathrm{I}}/\sigma\sqrt{\pi a}$ and $\overline{K}_{\mathrm{II}} = K_{\mathrm{II}}/\sigma\sqrt{\pi a}$.

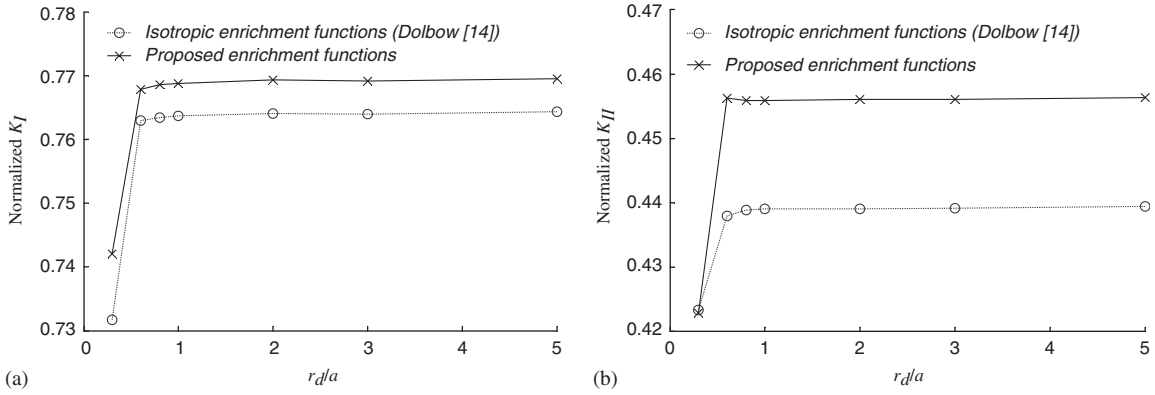

Fig. 14. Rate of convergence of SIFs with $\theta = 30°$ with respect to relative domain size in a plate with a slanted crack under remote tension for isotropic and proposed enrichment functions using 1496 elements: (a) normalized SIFs for mode I; (b) normalized SIFs for mode II. ($\overline{K}_{\mathrm{I}} = K_{\mathrm{I}}/\sigma\sqrt{\pi a}$ and $\overline{K}_{\mathrm{II}} = K_{\mathrm{II}}/\sigma\sqrt{\pi a}$).

in modes I and II, respectively, are at about 3.7% and 5% in the proposed method, and 0.6% and 1% for isotropic enrichment functions, all evaluated from the finest applied mesh. Also, the rate of convergence of normalized SIFs with $\theta = 30°$ with respect to the relative domain size is illustrated in Fig. 14, which shows almost similar rate of convergence for both enrichment functions.

4.3. An inclined center crack in a disk subjected to point loads

Geometry and boundary conditions of a disk subjected to point loads with an inclined crack are shown in Fig. 15. The whole view of FEM discretization is illustrated in Fig. 16 (a), whereas a detailed discretization around the crack–tips is shown in Fig. 16 (b). Eight hundred and fifty two four-noded elements with 877 nodes are used in the model. The material axes of orthotropy were assumed to be parallel to x_1- and x_2-axis and the following material properties were used in the finite element analysis

$$E_{11} = 0.1, \quad E_{22} = 1.0, \quad G_{12} = 0.5, \quad v_{12} = 0.03.$$

Stress intensity factors computed by the extended finite element analysis are compared with those reported by Kim and Paulino [18] for homogeneous orthotropic media for the case that θ=30°. Values of stress intensity factors for both modes are compared with two methods reported by Kim and Paulino [18] as provided in Table 6. They used 999 elements and 2712 nodes for their classic finite element crack simulation. For mode I,

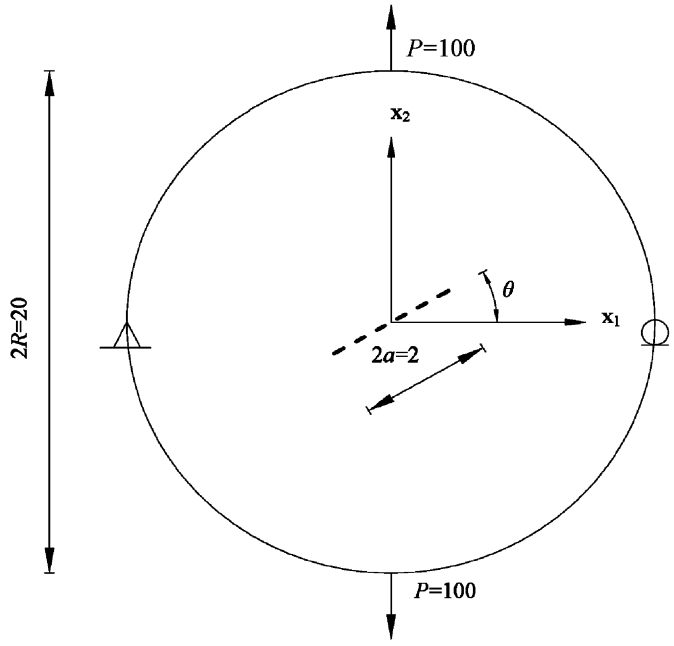

Fig. 15. Geometry and boundary conditions for an inclined center crack in a disk subjected to point loads.

the difference between stress intensity factors of the proposed method and Kim and Paulino [18] using M-integral is about 1.7%, whereas the difference slightly increases and reaches to about 2.4% for mode II.

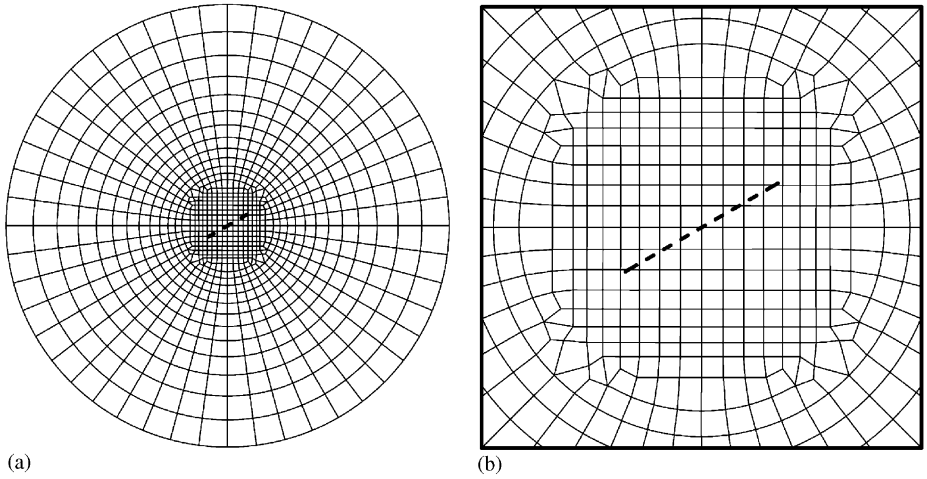

Fig. 16. FEM discretization for an inclined center crack in a disk subjected to point loads: (a) FEM discretization model; (b) details of discretization around the crack–tip.

Table 6
Values of stress intensity factors for an inclined center crack in a disk subjected to point loads; angle of crack alignment with respect to x_1-axis is $\theta = 30°$

Method		K_{I}	K_{II}
Kim and Paulino [18]	MCC	16.73	11.33
	M-integral	16.75	11.38
Proposed method		17.03	11.65

Fig. 17 illustrates stress intensity factors for various crack inclinations between 0° and 45°. The results show that while stress intensity factors decrease by increase of the crack inclination for mode I, they remain increasing for mode II. As mentioned in the example 2, only one finite element model is utilized for calculating all crack inclinations.

5. Conclusion

The problem of modeling crack in orthotropic media was studied. The extended finite element method was adopted for modeling the crack and analyzing the domain numerically. In the extended finite element method, first the finite element model without any discontinuities is created and then the two-dimensional asymptotic crack–tip displacement fields with a discontinuous function are added to enrich the finite element approximation using the framework of partition of unity. The main advantage is the ability of the method in taking into consideration the crack without any explicit meshing of the crack surfaces, and the growth of any crack can readily be applied without any remeshing. The analytical solution for the displacement is applied to obtain the two-dimensional asymptotic crack–tip functions. The proposed method considers only one group of orthotropic materials. The present method together

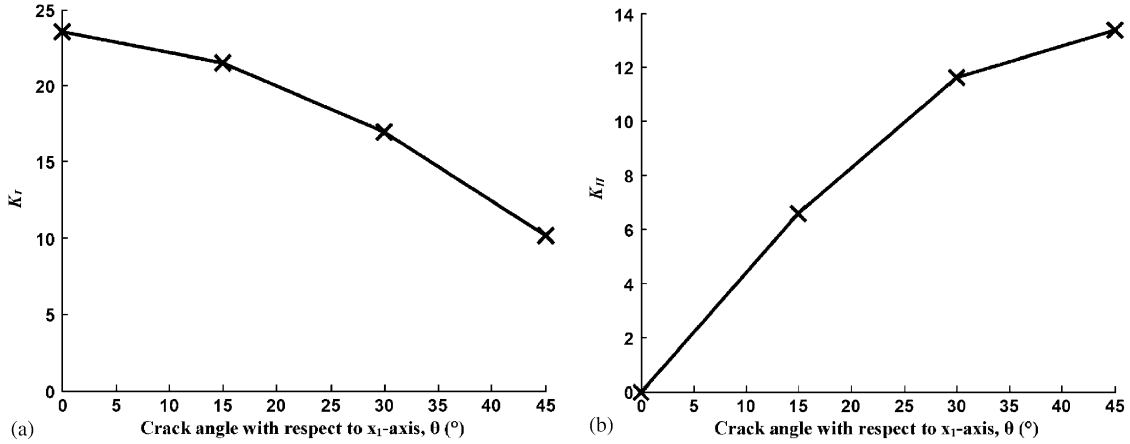

Fig. 17. Normalized SIFs corresponding to different crack angles of an inclined center crack in a disk subjected to point loads: (a) SIF for mode I; (b) SIF for mode II.

with the method proposed by Asadpoure et al. [17] cover all classes of orthotropic materials if the XFEM is to be applied for them. Mixed-mode stress intensity factors (SIFs) were evaluated to determine the fracture properties of domain. The results obtained by the proposed method are in good agreement with other available numerical or (semi-) analytical methods. In most examples, the maximum difference between the developed method and other available methods is about 1.7% for mode I and 2.4% for mode II. Numerical results depict that values of stress intensity factors are independent from the domain size as the domain size reaches to 0.325 of the crack length.

References

[1] N.I. Muskelishvili, Some Basic Problems on the Mathematical Theory of Elasticity, Noordhoof, Groningen, 1952.

[2] G.C. Sih, P.C. Paris, G.R. Irwin, On cracks in rectilinearly anisotropic bodies, Int. J. Fract. Mech. 1 (1965) 189–203.

[3] G.E. Tupholme, A study of cracks in orthotropic crystals using dislocations layers, J. Eng. Math. 8 (1974) 57–69.

[4] A. Viola, A. Piva, E. Radi, Crack propagation in an orthotropic medium under general loading, Eng. Fract. Mech. 34 (5) (1989) 1155–1174.

[5] W.K. Lim, S.Y. Choi, B.V. Sankar, Biaxial load effects on crack extension in anisotropic solids, Eng. Fract. Mech. 68 (2001) 403–416.

[6] L. Nobile, C. Carloni, Fracture analysis for orthotropic cracked plates, Compos. Struct. 68 (3) (2005) 285–293.

[7] T. Cruse, Boundary Element Analysis in Computational Fracture Mechanics, Kluwer, Dordrecht, 1988.

[8] D. Swenson, A. Ingraffea, Modeling mixed mode dynamic crack propagation using finite elements: theory and applications, Comput. Mech. 3 (1988) 381–397.

[9] T. Belytschko, Y.Y. Lu, L. Gu, Element-free Galerkin methods, Int. J. Numer. Meth. Eng. 37 (1994) 229–256.

[10] T. Belytschko, T. Black, Elastic crack growth in finite elements with minimal remeshing, Int. J. Numer. Meth. Eng. 45 (1999) 601–620.

[11] J.M. Melenk, I. Babuška, The partition of unity finite element method: basic theory and applications, Comput. Meth. Appl. Mech. Eng. 139 (1996) 289–314.

[12] C.A. Duarte, J.T. Oden, An H-p adaptive method using clouds, Comput. Meth. Appl. Mech. Eng. 139 (1996) 237–262.

[13] N. Moës, J. Dolbow, T. Belytschko, A finite element method for crack growth without remeshing, Int. J. Numer. Meth. Eng. 46 (1999) 131–150.

[14] J. Dolbow, An extended finite element method with discontinuous enrichment for applied mechanics, Ph.D. Thesis, Theoretical and Applied Mechanics, Northwestern University, Evanston, IL, USA, 1999.

[15] N. Sukumar, N. Moës, B. Moran, T. Belytschko, Extended finite element method for three-dimensional crack modeling, Int. J. Numer. Meth. Eng. 48 (2000) 1549–1570.

[16] N. Sukumar, J.-H. Prévost, Modeling quasi-static crack growth with the extended finite element method Part I: Computer implementation, Int. J. Solids Struct. 40 (2003) 7513–7537.

[17] A. Asadpoure, S. Mohammadi, A. Vafai, Crack Analysis in Orthotropic Media Using the Extended Finite Element Method, submitted for publication.

[18] J.H. Kim, G.H. Paulino, Mixed-mode fracture of orthotropic functionally graded materials using finite elements and the modified crack closure method, Eng. Fract. Mech. 69 (2002) 1557–1586.

[19] J.H. Kim, G.H. Paulino, The interaction integral for fracture of orthotropic functionally graded materials: evaluation of stress intensity factors, Int. J. Solids Struct. 40 (2003) 3967–4001.

[20] S.N. Atluri, A.S. Kobayashi, M.A. Nakagaki, Finite element program for fracture mechanics analysis of composite material, Fract. Mech. Compos. ASTM STP 593 (1975) 86–98.

[21] S.S. Wang, J.F. Yau, H.T. Corten, A mixed mode crack analysis of rectilinear anisotropic solids using conservation laws of elasticity, Int. J. Fract. 16 (1980) 247–259.